Composites Part B 270 (2024) 111110

Contents lists available at ScienceDirect

Composites Part B

journal homepage: www.elsevier.com/locate/compositesb

Mode II and mode III delamination of carbon fiber/epoxy composite laminates subjected to a four-point bending mechanism

S.I.B. Syed Abdullah [a], S.K. Bokti [b], K.J. Wong [c,*], M. Johar [d], W.W.F. Chong [b,e], Y. Dong [f]

[a] School of Mechanical Engineering, Engineering Campus, Universiti Sains Malaysia, 14300, Nibong Tebal, Pulau Pinang, Malaysia
[b] Faculty of Mechanical Engineering, Universiti Teknologi Malaysia, 81310, UTM Skudai, Johor, Malaysia
[c] Department of Mechanical Engineering, Faculty of Engineering and Science, Curtin University Malaysia, 98009, Miri, Malaysia
[d] Quality Engineering Research Cluster (QEREC), Quality Engineering Section, Malaysian Institute of Industrial Technology, Universiti Kuala Lumpur, 81750, Masai, Malaysia
[e] Automotive Development Centre, Institute for Vehicle Systems and Engineering (IVeSE), Universiti Teknologi Malaysia, 81310, Johor Bahru, Malaysia
[f] School of Civil and Mechanical Engineering, Curtin University, Perth, WA, 6845, Australia

ARTICLE INFO

Handling Editor: Prof. Ole Thomsen

Keywords:
Polymer-matrix composites (PMCs)
Laminate structures
Delamination
Fracture toughness
Finite element analysis (FEA)

ABSTRACT

Accurate determination of mode III interlaminar fracture toughness is paramount in composite materials due to its critical role in edge delamination, which nonetheless remains a significant challenge encountered. As such, this study focused on the investigation of mode II and III interlaminar fracture behavior of carbon fiber (CF)/epoxy composite laminates using four-end notched flexure (4ENF) tests and four-point bending plate (4PBP) tests, respectively. In particular, a cohesive zone model was employed for the simulation of the delamination process via finite element analysis (FEA). The mode II fracture toughness of CF/epoxy composites was determined to be 1.41 N/mm in experimental work. Additionally, experimental data in relation to force-displacement curves were in good agreement with numerical simulation results, which validated this simulation approach to successfully capture the mechanical response of composite laminates. In a similar manner, mode III delamination fracture toughness for CF/epoxy composites was numerically estimated to be 2.1 N/mm. Microscopic analysis indicated shear cusps were observed in both mode II and III specimens, as opposed to existing flakes discovered in mode III specimens only. Overall, this research enlightens a simple and effective way to estimate pure mode III fracture toughness and corresponding delamination behavior with respect to crack initiation and propagation.

1. Introduction

At present, the use of composite materials has seen a significant increase in various industries such as automobiles, aerospace, energy and marine engineering due to inherent high-strength-to-weight ratio, corrosion resistance and ease of manufacture of composite materials. Unfortunately, it is worth noting that composite materials are also susceptible to different types of mechanical damage comprised of matrix failure, fiber-matrix debonding, delamination and ultimately fiber failure. Among these, delamination is deemed as the most critical damage owing to its detrimental effect on the deterioration of load bearing capacity [1–4]. Consequently, it is vital to develop reliable methods for accurate prediction of edge delamination in a composite material system.

To date, the characterization of mode I, II and their mixed-mode interlaminar (delamination) failure is of a great concern in classical fiber composites reinforced with carbon fibers [5–7] and glass fibers [8]. Hosseini et al. [3,4] inserted mat layers at the delamination interface of twill woven glass/epoxy composites. Both initiation and steady-state fracture toughness of mat layers inserted into composites appeared to possess a decreasing trend under both mode I and II delaminations. Moreover, mode I delamination behavior was simulated using cohesive elements with different traction-separation law. The linear exponential law was found to be the best compared to superposed bilinear and exponential laws [3]. By conducting mode I and mode II delamination tests of woven carbon/epoxy composites in temperature range from −30 °C to 60 °C, Sabaghi et al. [9] reported that 175 thermal cycles deteriorated both initiation and steady-state fracture toughness of such composites. Finite element simulation using cohesive elements according to bilinear law was able to achieve good comparison between

* Corresponding author.
E-mail address: wongkingjye@curtin.edu.my (K.J. Wong).

https://doi.org/10.1016/j.compositesb.2023.111110
Received 27 July 2023; Received in revised form 14 October 2023; Accepted 20 November 2023
Available online 30 November 2023

experimental data and numerical results for force-displacement curves in relation to both mode I and mode II delamination. Bilinear law was also used to simulate debonding effect between Kevlar/polyester face-sheets and polyurethane foam core [10], which revealed a good agreement between experimental and numerical results for force-displacement curves.

On the other hand, testing approaches with respect to mode II fracture characterization consist of three-point end-notched flexure (3ENF) tests [11], end-loaded split (ELS) tests, as well as four-point end-notched flexure (4ENF) tests [12,13]. In particular, 4ENF tests are preferred owing to the robustness of such a testing method used in delamination propagation process [14].

As far as mode III delamination is concerned, there is not yet a standardized test despite the use of several testing techniques and methods for the characterization of mode III delamination fracture. These include split cantilever beam (SCB), simplified SCB (SSCB), modified SCB (MSCB), crack rail shear (CRS), anticlastic plate bending (ACPB), edge crack torsion (ECT), six ECT (6ECT), four-point bending plate (4PBP), shear torsion bending (STB) and split-shear torsion (SST) tests [15].

A study by de Morais and Pereira [16] summarized major challenges in effectively characterizing mode III fracture using existing methods. Initially, split cantilever beam (SCB) specimen was employed to measure critical strain energy release rate G_{IIIC} [17]. However, subsequent FEA revealed the presence of mode II components with unreliable results. Great attempts were made to modify SCB tests in order to eliminate spurious mode II effects though high stiffness of the specimens hindered the determination of accurate data reduction for mode III fracture toughness [18]. Similar issues were also observed in alternative crack rail shear (CRS) tests [19].

Nevertheless, recent advances enable to employ enhanced data reduction techniques for the purpose of accurate determination of initiation values of G_{IIIC} [20,21]. However, it was revealed that CF/epoxy composites possessed a typical behavior of substantial non-linearity prior to reaching the maximum load point, which induced a challenge to defining the initial point. With the existing difficulties associated with mode III fracture characterization, an alternative approach was adopted by means of 4PBP tests [16]. Despite 4PBP has a simple setup at the moderate cost, such a method is incapable of utilizing a data reduction method to facilitate the calculation of the G_{IIIC}. Instead it requires the alternative method of FEA for the prediction of G_{IIIC}. Nevertheless, it is worth noting that the reliability of the FE model is critical in numerical simulation work, which could be built based on a validated FE model with the adoption of similar test setup (four-point bending) using a data reduction method. In view of this, 4ENF is considered to be the best option. To our best knowledge, there is very limited work on using a validated 4ENF model to predict the G_{IIIC} and delamination behavior of 4PBP test. Due to a high demand to focus on the determination of pure mode III fracture toughness of composite materials using reliable and accurate testing methods, this study mainly investigated the evaluation of mode II and III delamination behavior for unidirectional (UD) CF/epoxy composite laminates.

In this present work, mode II and III fracture behavior were presented along with microstructural morphologies at failure. The deformation and failure of such composite materials were also numerically simulated with the aid of FEA using a cohesive zone model (CZM) under 4ENF and 4PBP mode II and III loadings, respectively. CZM was first validated by comparing the force-displacement response between the experimental result and the FE model established for the 4ENF specimen. Afterward, the same FEA methodology was implemented for the 4PBP specimen. The G_{IIIC} value was estimated by comparing the experimental and numerical force-displacement curves. The evolution of the crack growth in both 4ENF and 4PBP specimens was also presented and discussed. The findings from this study are expected to contribute to an overall understanding of delamination failure, leading to a simple and effective way to estimate the pure mode III fracture toughness and the corresponding delamination behavior.

2. Materials and methods

2.1. Materials and specimen geometry

CF/epoxy composite laminates used in this study were supplied by X-plas Singapore, which consisted of UD prepregs (nominal ply thickness: 0.15 mm). Average fiber diameter and fiber volume fraction were determined to be 6.8 μm and 65.7 ± 6.3 % [22]. A UD composite plate with a $[0]_{20}$ layup configuration was manufactured using the hand lay-up technique for 4ENF tests, as opposed to the fabrication of a 26-ply $[(90_2/0)_{2S}/0]_S$ composite laminate in the size of 500 × 420 mm^2 for 4PBP tests. To initiate the delamination process, a thin layer of polytetrafluoroethylene (PTFE) film (thickness: 15 μm) was inserted between plies at the mid-plane of both ends. Further curing process was carried out with a hot press machine for the consolidation of composite laminates with the thicknesses of 3.0 mm and 3.9 mm, respectively, in preparing the 4ENF and 4PBP specimens. Such laminates were allowed to cool down under ambient conditions. Finally, composite plates were cut into specimens by using a Computer Numerical Control (CNC) machine in the sizes of 155 × 20 and 155 × 68 mm^2 for 4ENF and 4PBP tests accordingly.

2.2. Mode II and mode III delamination test

Fig. 1(a) illustrates 4ENF test configuration for mode II delamination according to Martin and Davidson [13], as opposed to 4PBP tests in Fig. 1(b) in response to mode III delamination developed by de Morais and Pereira [16]. An Instron universal testing machine 5982, located at the Materials and Structures Laboratory, Universiti Teknologi Malaysia with a load cell capacity of 5 kN, was utilized for both tests at the crosshead speed of 1 mm/min. Fig. 2 shows the physical setup of the four-point bending test with the displacement applied vertically from the top. Initial crack lengths were set to 30 and 24 mm for 4ENF and 4PBP tests, respectively. To achieve good testing reproducibility, four specimens were used for 4ENF tests, as compared to three specimens for 4PBP tests.

2.3. Morphological characterization

A Scanning Electron Microscope (SEM) Hitachi Model S–3400 N was used to examine the fracture morphology of CF/epoxy composite laminates. Prior to that, delaminated surfaces were gold coated by Bio-Rad E5100 sputter coater to avoid negative surface charging issues, as well as enhance the emission of secondary electrons [23].

2.4. Mode II data reduction

G_{IIC} was calculated using the compliance calibration method [12,13], shown in Eq. (1):

$$G_{IIC} = \frac{P_C^2}{2B}\left(\frac{dC}{da}\right) \tag{1}$$

where P_C is the critical load, B is the specimen width, and $\frac{dC}{da}$ is the slope obtained based on a least squares fit of the compliance dC, as a function of crack length a. In this study, a cubic compliance function was used:

$$C = C_2 a^3 + C_1 \tag{2}$$

in which C_2 and C_1 are obtained through the curve fitting of the $C - a^3$ plot. Additional specimens were tested at different crack lengths of 20, 25, 35 and 40 mm within the linear load-displacement region to generate the compliance plot.

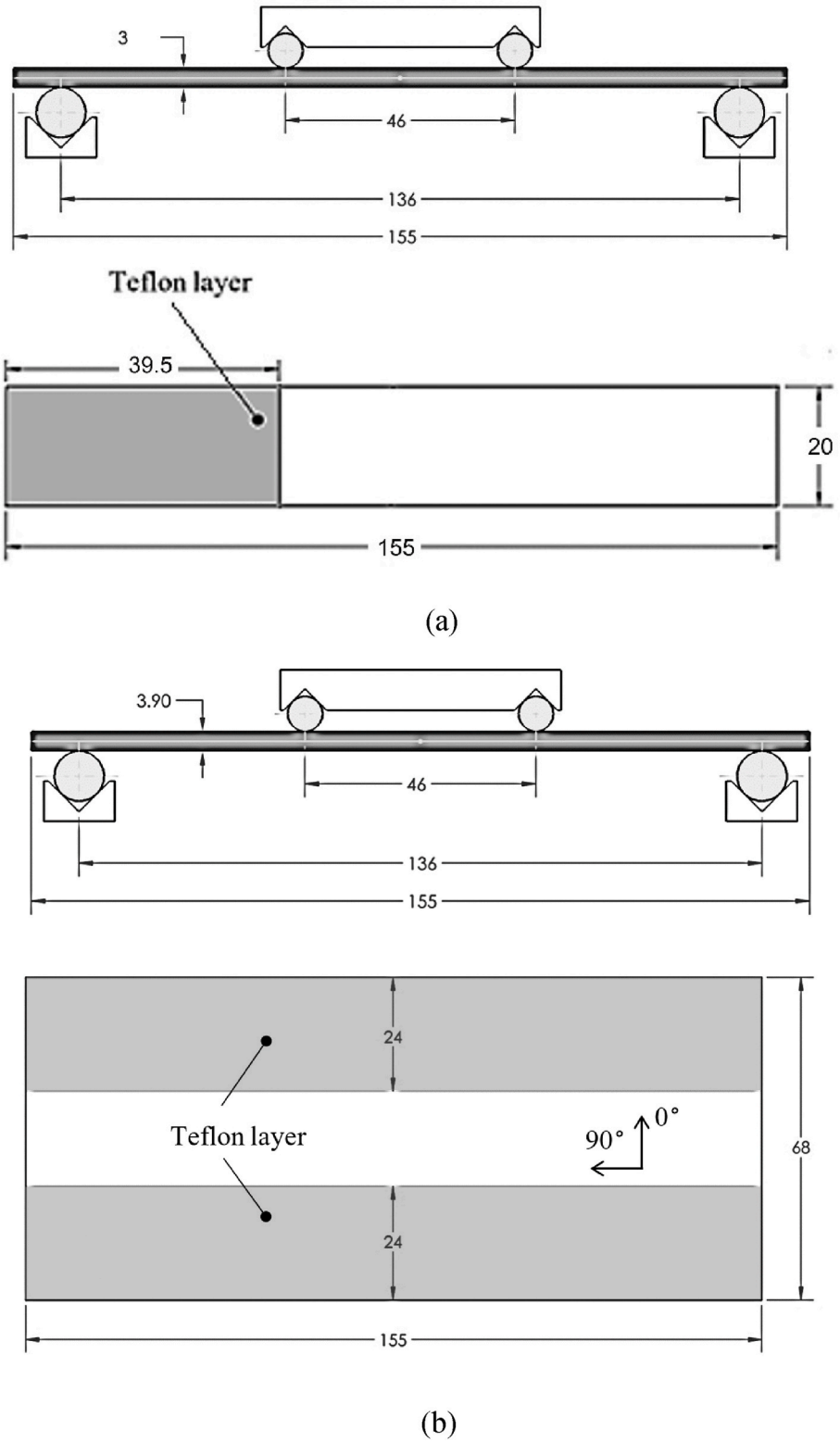

Fig. 1. Test setup and geometry of (a) 4ENF specimen and (b) 4PBP specimen (all dimensions are in mm).

3. Numerical modelling approach

3.1. Finite element models

Fig. 3 illustrates the finite element model of a 4ENF test specimen. The loading and boundary conditions were applied directly on the specimen at a distance as described in Fig. 3(a). The composite laminates were modeled using 8-node quadrilateral scheme in plane general-purpose continuum shell elements (SC8R). Since laminate damage is not simulated, the main concern in composite laminate modeling is to have accurate laminate properties, and to capture the bending behavior of composite materials. The laminate properties determined previously are listed in Table 1.

To represent the delamination behavior at the mid-plane interface,

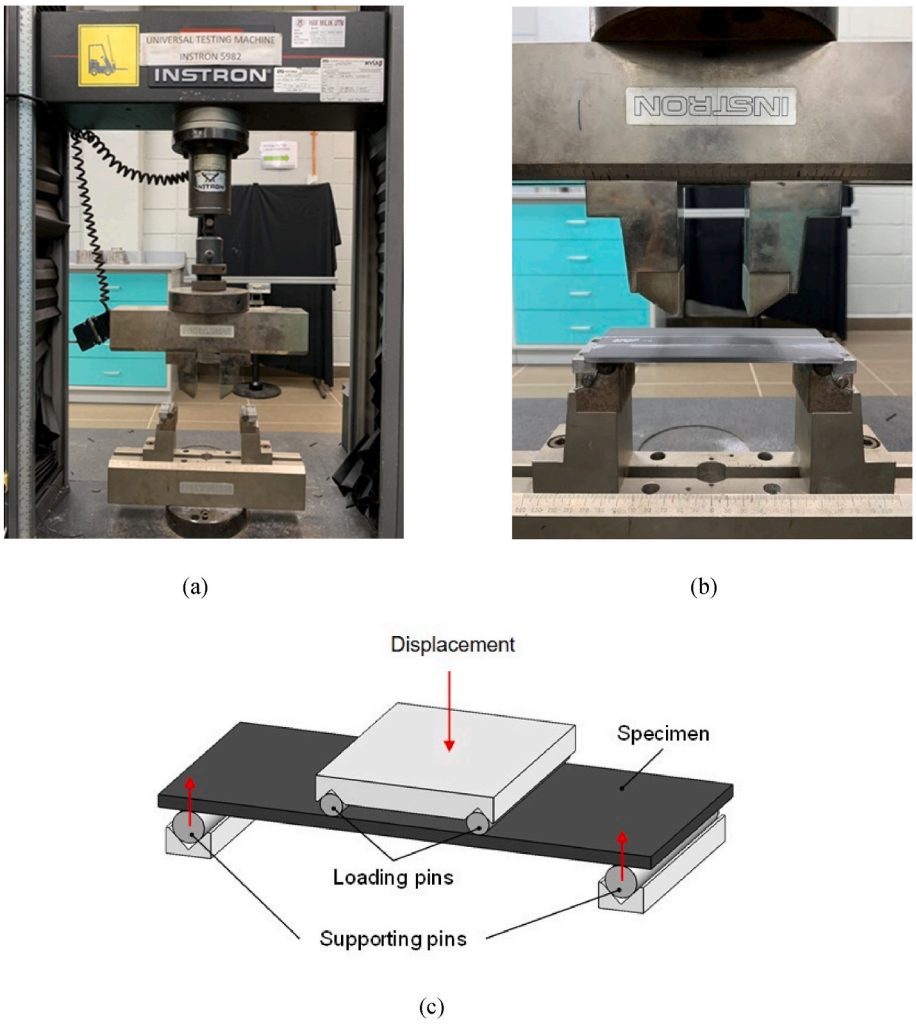

Fig. 2. Physical four-point bending test setup on an Instron 5982 universal testing machine: (a) without specimen; (b) with specimen in place; and (c) a loading mechanism.

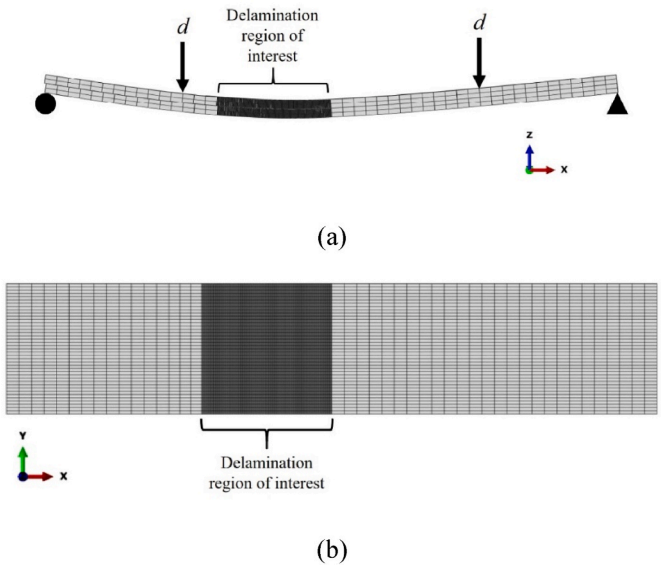

Fig. 3. Finite element model of a 4ENF specimen: (a) front view and (b) top view with the loading and boundary conditions.

Table 1
Mechanical properties for CF/epoxy composites used in this study [22,25].

Properties	Symbol	Value
Longitudinal elastic modulus	E_{11}	103 GPa
Transverse elastic modulus	E_{22}	6.7 GPa
In-plane shear modulus	G_{12}	2.7 GPa
Out-of-plane shear modulus	G_{13}	2.7 GPa
Out-of-plane shear modulus	G_{23}	2.5 GPa
In-plane Poisson's ratio	ν_{12}	0.24

cohesive elements in the form of 8-node three-dimensional cohesive elements (COH3D8) were employed. These cohesive elements were incorporated into the numerical simulation with a thickness of 10 μm to prevent any interpenetration issues [24]. Along the *x*-axis, the delamination region of interest was meshed with an element size of 0.1 mm to allow for the computation of accurate strain energy release rate [16]. In comparison, the remaining region was coarsely meshed with an element size of 2 mm. In the width direction (*y*-axis), it was discretized into an element size of 0.5 mm. Four elements were discretized in the thickness direction, which has been shown to sufficiently capture the bending behavior of identical composite materials under three-point bending [22,25]. Altogether the model was established based on a large quantity of 47,760 elements, in which 38,720 SC8R elements represented the composite laminate and 9040 COH3D8 elements denoted the

delamination interface. It is worth mentioning that finite element modeling was based on the same approach on the same material under 3ENF tests [22,25]. The comparison was carried out between 3D solid and continuum shell elements, and also the number of elements across the thickness direction of the specimen. In addition to that, the influence of the direct application of the loading and boundary conditions, when compared with that applied through rollers was also investigated. Apart from the direct comparison of force-displacement curves, a holistic analysis was conducted to ensure that the crack front stress field and crack propagation profile could be comparable. All finite element simulations were carried out using commercial ABAQUS software. The procedure type was *Static, General* with time period of 240 s and 600 s for 4ENF and 4PBP models, respectively. To ensure a reasonable amount of data to be captured, an increment size of maximum 1 s was set.

As for the 4PBP model, only a quarter specimen was modeled owing to the specimen geometry and lay-up symmetry to save computational time shown in Fig. 4. Specific loading and boundary conditions for this model are illustrated in Fig. 4(a) while the operation of symmetric boundary conditions to *x*- and *y*-planes of a quarter model is demonstrated in Fig. 4(b). Similar to a 4ENF specimen, composite laminate was modeled with SC8R elements while 10 μm-thick COH3D8 was employed to simulate the delamination along the mid-plane interface with the region of interest in element size of 0.5 × 0.5 mm^2. The outer region was meshed with a size of 1.5 mm in the *x*-axis direction. Four elements were discretized in the thickness direction. The 4PBP test was modeled using 41,888 elements, among which 39,168 SC8R type elements represented the composite laminate, and 2720 COH3D8 type elements were used for delamination interface.

3.2. Cohesive zone model

Cohesive elements were assigned to potential crack growth paths along an interface, and their behavior could be defined by the traction-separation law. Various traction-separation laws have been implemented, and custom-user subroutines can be integrated to handle cohesive elements with non-standard traction-separation laws [26]. A commonly used traction-separation law in numerical simulations is bilinear cohesive traction-separation law, which is very popular for its simplicity and adaptability. This model consists of an initial elastic region up to a full interface strength, followed by a softening region until a complete nodal pair separation is achieved at zero traction [27].

In Fig. 5, interfacial elements are characterized by several parameters including initial elastic stiffness K_i, cohesive strength $t_{u,i}$ and critical separation $\delta_{f,i}$. The subscript i denotes the degree of mode-mixity (i.e. pure mode II, mode III, or mixed mode II and III). When subjected to an opening traction t_i, the interface undergoes elastic opening with the initial stiffness until the traction reaches the cohesive interface strength ($t_i = t_{u,i}$) with a clear sign of damage initiation. The interface state is interpreted by a damage parameter D ranging from 0 to 1. The evolution of this damage parameter is governed by a specific damage evolution rule as follows:

$$D = \frac{\delta_{f,i}\left(\delta_i - \delta_{o,i}\right)}{\delta_i\left(\delta_{f,i} - \delta_{o,i}\right)} \tag{3}$$

where $\delta_{o,i} = t_{u,i}/K_i$ is corresponding separation for damage initiation and δ_i is instantaneous separation for the interface element. When the interface element is partially damaged ($0 < D < 1$), the opening stress is related to the opening displacement linearly given by:

$$t_i = (1 - D)\, K_i \delta_i \tag{4}$$

When combining Eq. (3) and Eq. (4), it is specified that the stress decreases linearly with the separation ($\delta_{o,i} < \delta_i \leq \delta_{f,i}$):

$$t_i = t_{u,i}\frac{\delta_{f,i} - \delta_i}{\delta_{f,i} - \delta_{o,i}} \tag{5}$$

when $\delta \geq \delta_{f,i}$, $D = 1$ and $t_i = 0$, the interface element is fully damaged.

As seen from Fig. 5, fracture energy G_{iC} can also be defined as

$$G_{iC} = \frac{1}{2} t_{u,i} \delta_{f,i} \tag{6}$$

Note that penalty stiffness $K_i = 4.5 \times 10^5$ MPa/mm was used for both mode II and III in this study [22,25].

4. Results and discussion

4.1. Experimental mode II force-displacement curves

Fig. 6 presents the compliance plots of 4ENF tests. Note that the best

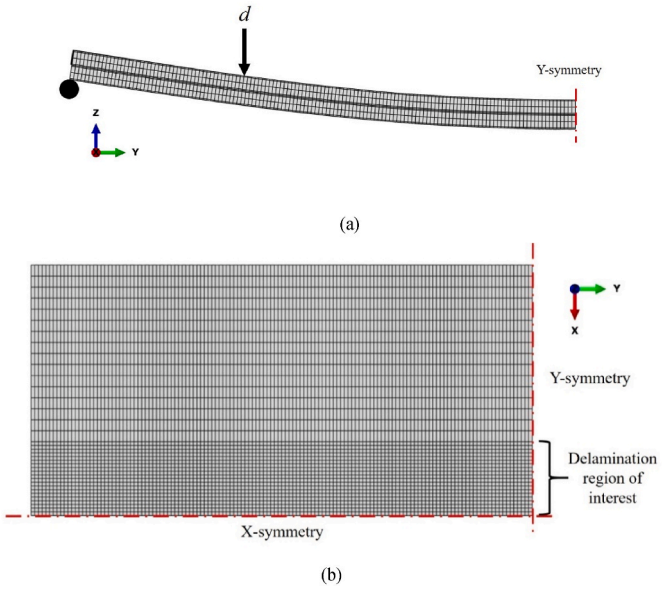

Fig. 4. Finite element model of a 4PBP specimen: (a) a front view with the loading and boundary conditions and (b) a top view to illustrate symmetric boundary conditions.

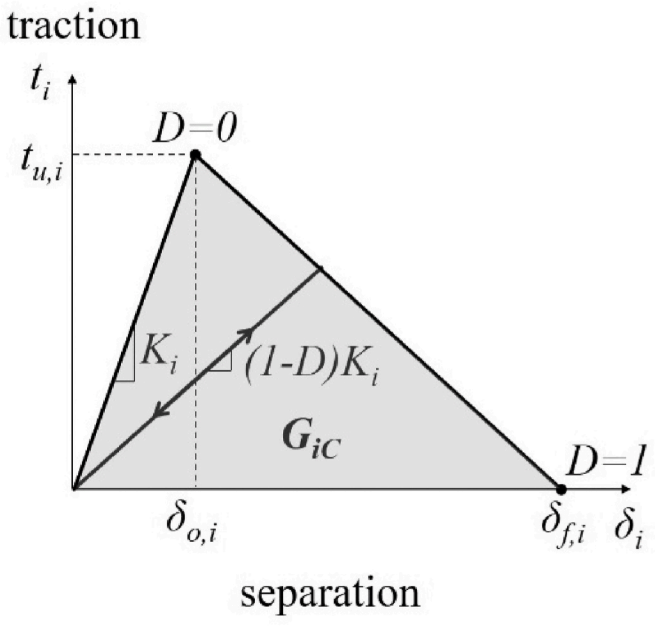

Fig. 5. Bilinear traction-separation law for pure mode delamination.

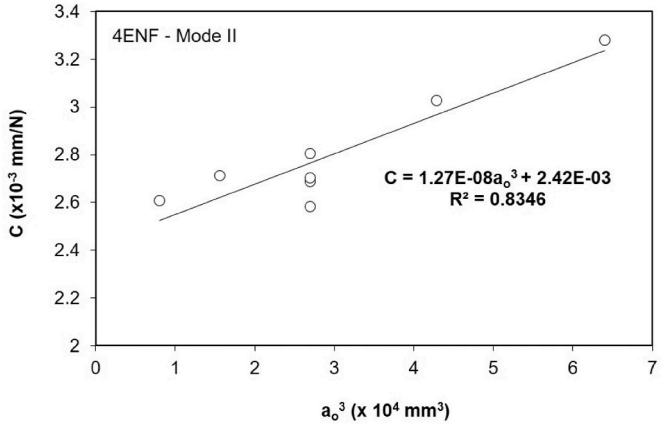

Fig. 6. Compliance plot of mode II 4ENF test.

fit parameters are also included in Fig. 6. Mode II force-displacement curves for CF/epoxy composite laminates are depicted in Fig. 7 where an obvious dramatic drop can be seen upon reaching the peak force, indicating delamination initiation.

The average initiation G_{IIC} was determined to be 1.41 ± 0.16 N/mm (CV: 11 %), which is consistent with the previous work by Low et al. [22] based on the same composite material. Note that the result is also consistent with previous results for a similar testing method and composite configuration [14,28]. It should be noted that the effect of friction was negligible in this case in accordance with [29–31]. Alternatively, the mode II interfacial strength can be determined using Eq. (7) [32], as shown below:

$$t_{u,s} = \sqrt{\frac{G_{IIC}}{G_{IC}}} t_{u,n} \tag{7}$$

where $t_{u,n}$ is the normal interfacial strength (mode I), $t_{u,s}$ is the shear interfacial strength (mode II), G_{IC} and G_{IIC} refer to the mode I and mode II fracture toughness, respectively. Using Eq. (7), the mode II interfacial strength was calculated to be $t_{u,s} = 84$ MPa, along with $t_{u,n} = 35$ MPa and $G_{IC} = 0.245$ N/mm, as reported by Low et al. [33] for a UD CF/epoxy composite laminate, which was the same material used in this study.

4.2. Experimental mode III force-displacement curves

Fig. 8 shows the force-displacement curves obtained from the mode III 4PBP tests. Similar to the 4ENF tests, the force in 4PBP tests increases linearly up to the peak load of approximately 3 kN, following which a sudden drop can be observed indicating crack Mode II crack initiation at the initial stage. Note that all specimens displayed a similar force-

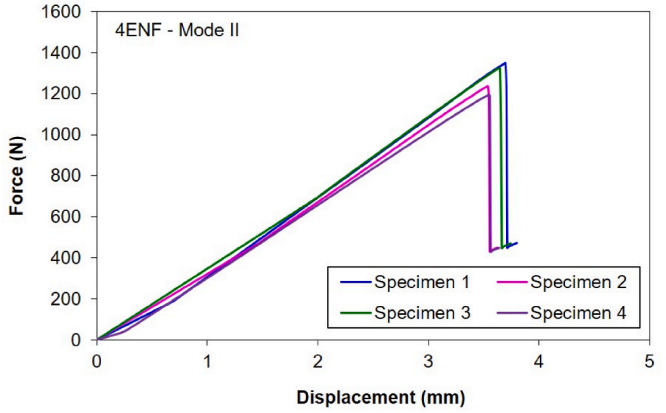

Fig. 7. Mode II experimental force–displacement curves in 4ENF tests.

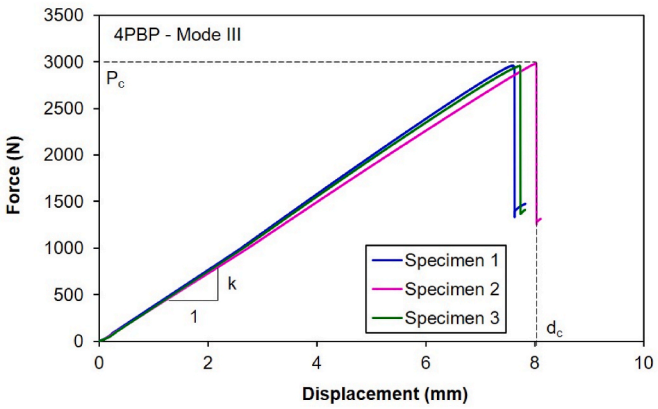

Fig. 8. Mode III force–displacement curves in 4PBP tests. An example of the definition of P_C, k and d_C is labeled on Specimen 2.

displacement response. Table 2 presents the peak force P_C, slope k (within the force range of 1000–2000 N), as well as corresponding crosshead displacement d_C when peak force was attained.

4.3. Mode II morphological analysis

One of essential fractographic features in a mode II-dominated failure is shear cusps, which appear on the fracture surfaces as inclined platelets [34]. A larger (or thicker) cusp size can be detected depending on some factors such as fiber volume fraction. In addition, the morphology of the cusps could also provide insight to the direction of crack growth [34]. As illustrated in Fig. 9, the cusps formation is generally small, which implies that composite laminates have a relatively high fiber volume fraction as well as minimal resin-rich area in each laminate. In general, shear cusps are attributed to the relative movement of upper and lower surfaces leading to matrix cleavage [35]. In addition, the inclination of shear cusps also plays an essential role in determining the shearing direction. When the shear cusps are inclined to the left, the shearing direction may tend to move from the left to the right by assumption [34].

Furthermore, fiber imprints are observed particularly near matrix-dominant areas, as well as the residues of broken fibers on fracture surfaces according to Fig. 9. Such imprints suggest that mechanical failure prevalently occurs at the fiber/matrix interface under mode II loading. As such, clean fiber tracks remain on the matrix-dominant side of fracture surfaces where those fibers could often be found to be stripped of the matrices with small-sized cusps scattering around fracture surfaces. It should be evident that final G_{IIC} of composite laminates can be influenced by matrix cracking, fiber-matrix debonding, as well as further fiber failure [36].

4.4. Mode III morphological analysis

Fig. 10 presents the fractographic images of delaminated surfaces under mode III loading. The presence of broken fiber ends is manifested, which suggests that fiber bridges may be generated between fracture surfaces in good accordance with Bertorello et al. [37]. Additionally, the

Table 2
Data summary of mode III 4PBP tests.

Specimen No.	P_C (N)	k (N/mm)	d_C (mm)
1	2957.46	413.23	7.83
2	2982.95	388.87	8.11
3	2955.07	406.98	7.83
Average	2965.16	403.03	7.93
S.D	15.45	12.65	0.16
C.V (%)	0.52	3.14	2.05

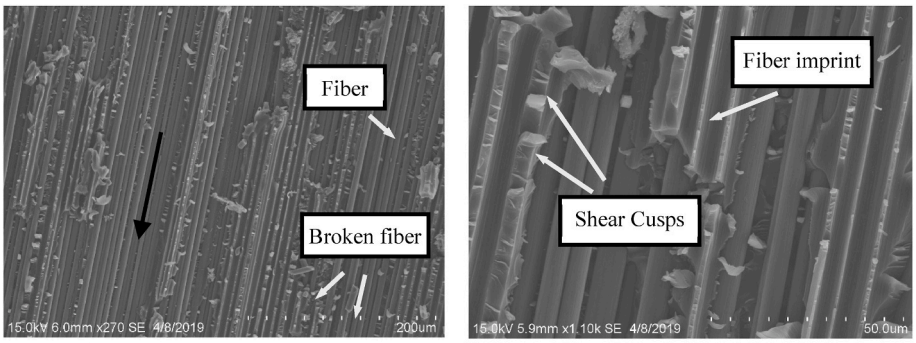

(a) (b)

Fig. 9. (a) Fracture surface of CF/epoxy composite laminate under a mode II loading (Black arrow indicates the shearing direction) and (b) Close-up view of the fracture surface.

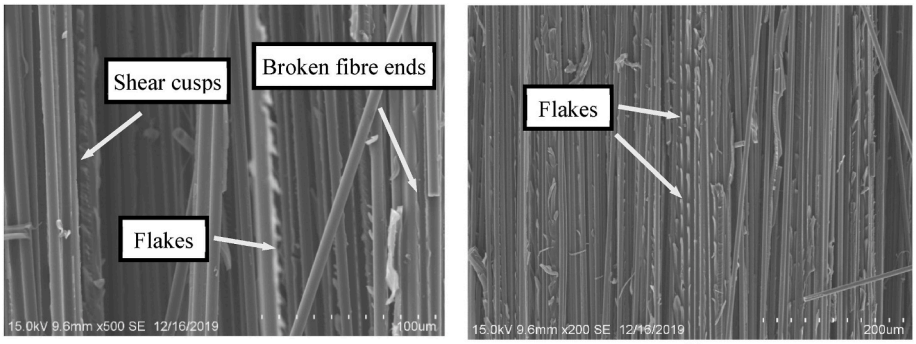

(a) (b)

Fig. 10. Scanning electron micrographs of the mode III 4-PBP specimen.

existence of flakes is indicative of a typical saw-teeth feature [38,39] in mode III failure. The flakes appear to be oriented at an angle of 45° with respect to the fiber axis in the specimens as a result of dominant tangential stresses acting in the fiber direction or perpendicular to their orientation. Because of such a stress distribution, main stresses are aligned with the bisector of the angle formed in the fiber direction [37]. Shear cusps observed can be taken as the indicator of typical mode III fracture characteristic [39,40].

4.5. Mode II finite element analysis

Fig. 11 presents typical force-displacement response obtained from numerical simulation with the comparison of experimental data. In general, finite element model is demonstrated with good prediction to experimental data for most of force-displacement curves with the maximum error being less than 7 %, thus proving the validity of developed numerical model in this finite element approach.

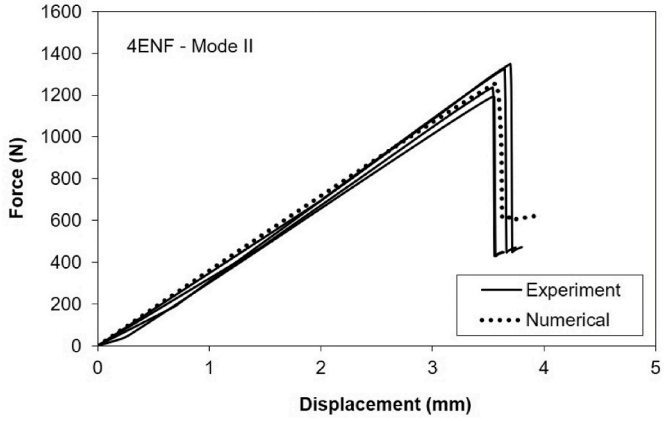

Fig. 11. Experimental and numerical comparison of force-displacement curves in 4ENF tests.

Fig. 12 characterizes the crack growth when peak force is acquired. Due to the symmetric crack growth profile with respect to the width direction, only a half of the specimen is shown. The mid-width location is labeled *y*-symmetry where the crack is extended by 5.6 mm. The crack extension across the width exhibits a distinctively reversed thumb-like pattern with slightly faster propagation at the free edge with the crack extension by 6 mm.

4.6. Determination of mode III strain energy release rate G_{IIIC}

A range of G_{IIIC} values were selected and numerical results were well compared with experimental data to be in good agreement with experimental load-displacement curves obtained in mode III tests. Initial G_{IIIC} values were estimated from previous studies on mode III characterization of UD CF/epoxy laminates [16,41]. Table 3 lists numerical results using five different G_{IIIC} values in an input range of 2.0–2.2 N/mm. It should be noted that mode III interface strength $t_{u,t}$ is estimated according to Eq. (8) below, which is similar to mode II based on Eq. (7).

$$t_{u,t} = \sqrt{\frac{G_{IIIC}}{G_{IC}}} t_{u,n} \tag{8}$$

where $t_{u,n}$ is the mode I interfacial strength, and $t_{u,t}$ is the mode III interfacial strength. G_{IC} and G_{IIIC} indicate the mode I and mode III fracture toughness, respectively.

This means that corresponding mode III interface strength is suggested to be adjusted according to each estimated G_{IIIC}. The subscript *t*

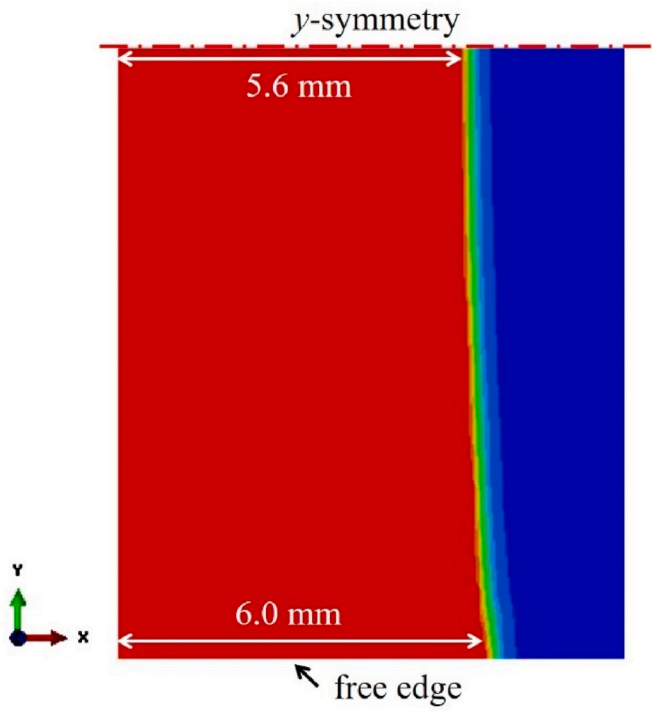

Fig. 12. Crack growth profile at the peak force for a 4ENF specimen.

refers to the tearing mode, commonly known as mode III delamination. In Table 3, the maximum error refers to the most significant difference among the three specimens listed in Table 2. It was found that $G_{IIIC} = 2.1$ N/mm yielded the experimental peak force with the best correlation where the numerical peak force of 2940.80 N was kept to be lower when compared with corresponding experimental data. The numerical peak force was chosen to be the closest, but lower than the experimental counterpart for the purpose of conservative numerical prediction. The relevant numerical k of 388.22 N/mm and d_C of 7.54 mm are also well compared with experimental data, resulting in maximum errors obtained only up to approximately 6 % and 7 %, respectively. It should be noticed that bilinear cohesive formulation does not take any fiber-bridging effect into account, which may contribute to actual experimental fracture toughness. Fig. 13 exhibits experimental and numerical force-displacement curves in 4PBP tests. Moreover, the analytically derived compliance curve from a simple beam theory relationship [42] is used for comparison.

In case of mode III, though the test method currently selected requires FEA to predict G_{IIIC}, it can be considered as a faster and more cost-effective method, as opposed to other testing methods depending on extensive sample preparation. Apparently, G_{IIIC} obtained in this study coincides with those detected in other studies with a similar configuration of composite materials [16,41].

Crack propagation of cohesive element along the x-axis and y-axis were measured at three different instances: i) when the first element reaches the interface strength, which is indicated as D = 0 in Fig. 5; ii) when the first element reaches total failure, labeled D = 1 in Fig. 5; and iii) when the peak force is attained. The corresponding crosshead displacement in these three instances is also labeled in Fig. 13, including 1.8, 5.5 and 7.5 mm. Fig. 14 shows the respective crack growth contour at the three selected instances. The same delamination region of interest shown in Fig. 4(b) is taken into consideration. Fig. 14(a) reveals that the crack is initiated at the edge of the crack front. This is consistent with the observation reported in Ref. [16]. Subsequently, crack propagation takes place along both x and y axes undergoing a faster rate in the y-axis (43.5 mm), as compared to the x-axis (1 mm) according to Fig. 14(b). At the peak force, Fig. 14(c) shows that the lengths of crack propagation along the y-axis and the x-axis were determined to be 47.5 and 2.0 mm, respectively.

5. Further discussion

G_{IIC} values were very similar at 1.41 and 1.35 N/mm for 4ENF tests and 3ENF tests [22] despite admittedly significant disparity taking place in predicted crack extension at the peak force via FEA. From the FEA results, 4ENF specimen had a mid-width crack growth of 5.6 mm, as opposed to the extension of 3.8 mm for a 3ENF specimen with a remarkable difference of approximately 50 %. The specific methodology used for validated 4ENF model was also implemented for 4PBP model, resulting in an estimated average G_{IIIC} of 2.1 N/mm. It further led to the ratio of mode III to mode II fracture toughness G_{IIIC}/G_{IIC} at 1.49. In contrast, G_{IIIC}/G_{IIC} ratio for UD CF/epoxy composite laminates was determined to be 1.94 by de Morais and Pereira [16] where $G_{IIC} = 0.8$ N/mm and $G_{IIIC} = 1.55$ N/mm. It is worth noting that predicted G_{IIC} of 1.55 N/mm in 4PBP model becomes higher when compared with that characterized by ECT tests in a range of 0.85–1.1 N/mm [20]. As a whole, it can be concluded that mode III strain energy release rate exceeds mode II counterpart in spite of the variation of G_{IIIC} values acquired from different testing methods.

6. Conclusions

Current work presents a holistic characterization of mode II and III

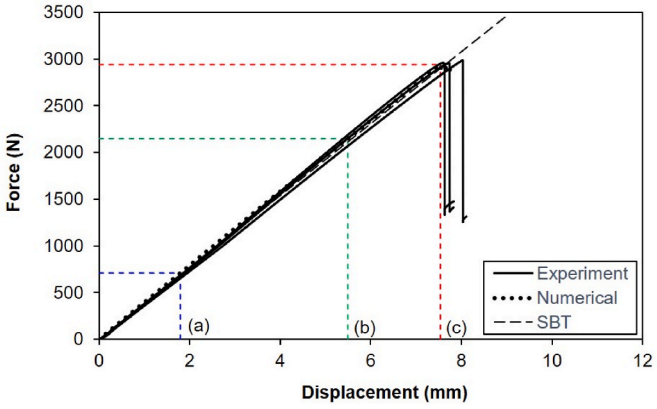

Fig. 13. Experimental and numerical comparison with respect to force–displacement curves for $G_{IIIC} = 2.1$ N/mm given in the cohesive zone model.

Table 3
Data summary for the load-displacement curves based on G_{IIIc} inputs using cohesive zone damage model.

G_{IIIC} (N/mm)	$t_{u,t}$ (MPa)	P_C (N)	Max % difference	k (N/mm)	Max % difference	d_C (N)	Max % difference
2	100	2890.79	3.09	387.13	6.32	7.41	8.65
2.05	101	2915.87	2.25	387.68	6.18	7.47	7.86
2.1	102	2940.80	1.41	388.22	6.05	7.54	7.08
2.15	104	2984.98	−0.07	389.59	5.72	7.65	5.70
2.2	105	3009.23	−0.88	390.13	5.59	7.71	4.94

Note: Negative means that the experimental value is lower than the numerical counterpart.

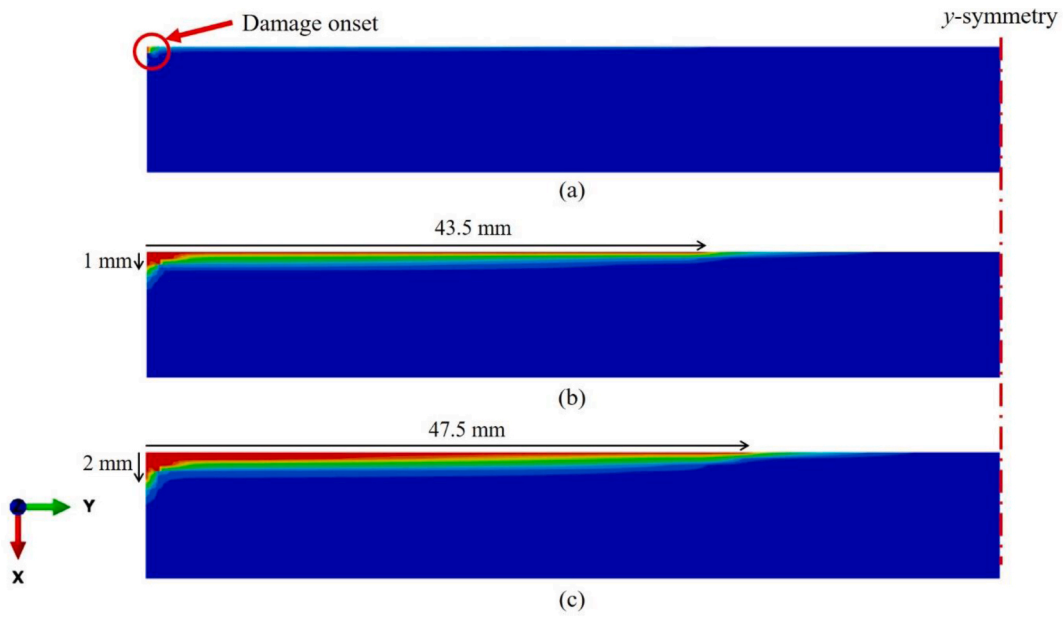

Fig. 14. Crack propagation at the peak force for a 4PBP specimen.

fracture toughness in CF/epoxy composites based on a combination of experimental and numerical techniques using four-point bending test. Mode II delamination test was carried out using four-point end notched flexure (4ENF) test, while mode III delamination was conducted using four-point bending plate (4PBP) test. All tests were conducted at the crosshead speed of 1 mm/min in ambient conditions. The surface morphology was characterized via scanning electron microscopy. In addition, the delamination behavior of both specimen types was systematically simulated via finite element analysis using cohesive elements according to bilinear traction-separation law.

Mode II delamination behavior was indicative of an average G_{IIC} value of 1.41 N/mm in 4ENF tests, which was well aligned with that obtained in 3ENF tests. The presence of shear cusps in microstructural morphology suggested that such a characteristic fracture behavior could be related to mode II loading failure.

As for mode III delamination in 4PBP tests, it appeared that flakes were identified on fracture surfaces with a clear sign of tearing effect in addition to shear cusps, thus resulting in a complex fracture mechanism for mode III delamination. Numerical results obtained using FEA demonstrated a predicted G_{IIIC} value of 2.1 N/mm.

With the presence of distinctive fracture behavior associated with various mode II or III fracture toughness values, it can be clearly demonstrated that this study contributes to the simple setup at moderate cost for pure mode II and mode III characterization, as well as the delamination behavior simulation through reliable finite element models using cohesive elements.

Author statement

K. J. Wong: Corresponding author.
S. I. B. Syed Abdullah: Co-author.
S. K. Bokti: Co-author.
M. Johar: Co-author.
W. W. F. Chong: Co-author.
Y. Dong: Co-author.

Declaration of competing interest

The authors declare that they have no known competing financial interests or personal relationships that could have appeared to influence the work reported in this paper.

Data availability

Data will be made available on request.

Acknowledgements

This research project received financial support from the Ministry of Higher Education (MOHE) Malaysia under the Fundamental Research Grant Scheme (FRGS) with the reference number FRGS/1/2023/TK10/UTM/02/3 and Universiti Teknologi Malaysia under the UTM Fundamental Research (UTMFR) with reference number Q.J130000.3851.22H02.

References

[1] Garg AC. Delamination - a damage mode in composite structures. Eng Fract Mech 1988;29(5):557–84.
[2] Wisnom MR. The role of delamination in failure of fibre-reinforced composites. Philosophical Transactions of the Royal Society A 2012;370(1965):1850–70.
[3] Hosseini MR, Taheri-Behrooz F, Salamat-talab M. Mode I interlaminar fracture toughness of woven glass/epoxy composites with mat layers at delamination interface. Polym Test 2019;78:105943.
[4] Hosseini MR, Taheri-Behrooz F, Salamat-talab M. Mode II interlaminar fracture toughness of woven E-glass/epoxy composites in the presence of mat interleaves. Int J Adhesion Adhes 2020;98:102523.
[5] Gong Y, Chen X, Li W, Zhao L, Tao J, Zhang J, Hu N. Delamination in carbon fiber epoxy DCB laminates with different stacking sequences: R-curve behavior and bridging traction-separation relation. Compos Struct 2021;262:1–13.
[6] Yu G, Linfei J, Linkang L, Zhao J. An experimental and numerical study of the influence of temperature on mode II fracture of a T800/epoxy unidirectional laminate. Materials 2022;15(12):1–19.
[7] Pereira AB, de Morais AB. Mixed mode I + II interlaminar fracture of carbon/epoxy laminates. Compos Appl Sci Manuf 2008;39(2):322–33.
[8] Samborski S, Gliszczynski A, Rzeczkowski J, Wiacek N. Mode I interlaminar fracture of glass/epoxy unidirectional laminates. Part I: experimental studies. Materials (Basel) 2019;12(10):1–12.
[9] Sabaghi M, Taheri-Behrooz F, Salamat-Talab M. Critical strain energy release rate of woven carbon/epoxy composites subjected to thermal cyclic loading. Polym Compos 2022;43(9):6135–49.
[10] Gholami V, Taheri-Behrooz F, Memar Maher B. Fracture toughness and crack growth resistance of sandwich panels with grooved cores. J Sandw Struct Mater 2022;24(3):1746–67.
[11] Low KO, Johar M, Israr HA, Gan KW, Koloor SSR, Petru M, Wong KJ. Displacement rate effects on the mode II shear delamination behavior of carbon fiber/epoxy composites. Polymers 2021;13(1881):1–18.
[12] Robinson P, Hodgkinson JM. Interlaminar fracture toughness. In: Mechanical testing of advanced fibre composites. Cambridge, England: Woodhead Publishing Limited; 2000. p. 170–210.

[13] Martin RH, Davidson BD. Mode II fracture toughness evaluation using a four point bend end notched flexure test. Plast, Rubber Compos 1999;28(8):401–6.
[14] Wang W-X, Nakata M, Takao Y, Matsubara T. Experimental investigation on test methods for mode II interlaminar fracture testing of carbon fiber reinforced composites. Compos Appl Sci Manuf 2009;40(9):1447–55.
[15] López-Menéndez A, Viña J, Argüelles A, Rubiera S, Mollón V. A new method for testing composite materials under mode III fracture. J Compos Mater 2016;50(28):3973–80.
[16] de Morais AB, Pereira AB. Mode III interlaminar fracture of carbon/epoxy laminates using a four-point bending plate test. Compos Appl Sci Manuf 2009;40(11):1741–6.
[17] Donaldson SL. Mode III interlaminar fracture characterization of composite materials. Compos Sci Technol 1988;32(1988):225–49.
[18] Song PRaDQ. The development of an improved mode III delamination test for composites. Compos Sci Technol 1994;52:217–33.
[19] Becht Gary, John W, Gillespie J. Design and analysis of the crack rail shear specimen for mode III interlaminar fracture. Composttes Scwnce and Technology 1988;(31):143–57.
[20] de Morais AB, Pereira AB, de Moura MFSF, Magalhães AG. Mode III interlaminar fracture of carbon/epoxy laminates using the edge crack torsion (ECT) test. Compos Sci Technol 2009;69(5):670–6.
[21] Moura, M.F.S.F.d., Numerical analysis of the Edge Crack Torsion test for mode III interlaminar fracture of composite laminates.
[22] Low KO, Johar M, Israr HA, Gan KW, Rahimian Koloor SS, Petrů M, Wong KJ. Displacement rate effects on the mode II shear delamination behavior of carbon fiber/epoxy composites. Polymers 2021;13(11).
[23] Leslie SA, Mitchell JC. Removing gold coating from sem samples. Palaeontology 2007;50(6):1459–61.
[24] Sørensen BF, Goutianos S, Jacobsen TK. Strength scaling of adhesive joints in polymer–matrix composites. Int J Solid Struct 2009;46(3–4):741–61.
[25] Wong KJ, Johar M, Koloor SS, Petrů M, Tamin MN. Moisture absorption effects on mode II delamination of carbon/epoxy composites. Polymers 2020;12(9).
[26] Haixia Mei SG, Liechti Kenneth M, Huang Rui. Initiation and propagation of interfacial delamination in integrated thin-film structures. IEEE; 2010.
[27] Li G, Li C. Linking bilinear traction law parameters to cohesive zone length for laminated composites and bonded joints. Advances in aircraft and spacecraft science 2014;1(2):177–96.
[28] Franklin VA, Christopher T. Generation of R-Curve from 4ENF specimens: an experimental study. Journal of Composites 2014;2014:1–11.
[29] Schuecker C, Davidson BD. Effect of friction on the perceived mode II delamination toughness from three- and four-point bend end-notched flexure tests. West Conshohocken, PA: American Society for Testing and Materials (ASTM); 2000.
[30] Mencattelli L, Borotto M, Cugnoni J, Lazzeri R, Botsis J. Analysis and evaluation of friction effects on mode II delamination testing. Compos Struct 2018;190:127–36.
[31] Ballarin P, Airoldi A, Aceti P, Ghiasvand S, Sala G. Experimental identification of frictional effects on interlaminar toughness of composite laminates in 4ENF test. Exp Mech 2022;62:1135–45.
[32] Turon A, Camanho PP, Costa J, Renart J. Accurate simulation of delamination growth under mixed-mode loading using cohesive elements: definition of interlaminar strengths and elastic stiffness. Compos Struct 2010;92(8):1857–64.
[33] Low KO, Teng SM, Johar M, Israr HA, Wong KJ. Mode I delamination behaviour of carbon/epoxy composite at different displacement rates. Compos B Eng 2019;176:107293.
[34] Greenhalgh ES. Delamination-dominated failures in polymer composites. In: Failure analysis and fractography of polymer composites. Cambridge: Woodhead Publishing Limited; 2009. p. 164–237.
[35] Barbosa LCM, Souza SDB, Botelho EC, Candido GM, Rezende MC. Fractographic study of welded joints of carbon fiber/PPS composites tested in lap shear. Eng Fail Anal 2018;93:172–82.
[36] Hull D, Clyne TW. Toughness of composites. In: An introduction to composite materials. Cambridge: Cambridge University Press; 1996. p. 208–36.
[37] Bertorello C, Vina J, Vina I, Arguelles A. Study of the influence of the type of matrix used in carbon-epoxy composites on fatigue delamination under mode III fracture. Mater Des 2020;186:1–7.
[38] Bertorello C, Arguelles A, Mollon V, Bonhomme J, Vina I, Vina J. Use of a LHFB device for testing mode III in a composite laminate. Polymers 2019;11:1–9.
[39] Lopez M, Vina AJ, Arguelles A, Lozano M. Validation of the longitudinal half fixed beam method for characterizing mode III delamination of composite materials. Compos Struct 2016;147:74–81.
[40] Li X, Carlsson A, Davies P. Influence of fiber volume fraction on mode III interlaminar fracture toughness of glass/epoxy composites. Compos Sci Technol 2004;69:1279–86.
[41] de Morais AB, Pereira AB, de Moura MFSF. Mode III interlaminar fracture of carbon/epoxy laminates using the Six-Point Edge Crack Torsion (6ECT). Compos Appl Sci Manuf 2011;42(11):1793–9.
[42] Robinson P, Hodgkinson JM. 9 - interlaminar fracture toughness. In: Hodgkinson JM, editor. Mechanical testing of advanced fibre composites. Woodhead Publishing; 2000. p. 170–210.